RESEARCH PAPER

How do cryptochromes and UVR8 interact in natural and simulated sunlight?

Neha Rai[1,*], Susanne Neugart[2], Yan Yan[1], Fang Wang[1], Sari M. Siipola[1], Anders V. Lindfors[3], Jana Barbro Winkler[4], Andreas Albert[4], Mikael Brosché[1], Tarja Lehto[5], Luis O. Morales[1,†,‡] and Pedro J. Aphalo[1,‡]

[1] Organismal and Evolutionary Biology Research Programme, Viikki Plant Science Center, University of Helsinki, 00014 Helsinki, Finland
[2] Research Area of Plant Quality and Food Security, Leibniz Institute of Vegetable and Ornamental Crops e. V., 14979 Grossbeeren, Germany
[3] Finnish Meteorological Institute, FI-00101 Helsinki, Finland
[4] Research Unit Environmental Simulation, Helmholtz Zentrum München, Ingolstädter Landstrasse 1, D-85764 Neuherberg, Germany
[5] School of Forest Sciences, University of Eastern Finland, FI-80101 Joensuu, Finland

[†] Current address: School of Science & Technology, Örebro Life Science Center, Örebro University, SE-70182 Örebro, Sweden
[‡] Joint senior authors.
*Correspondence: neha.rai@helsinki.fi

Abstract

Cryptochromes (CRYs) and UV RESISTANCE LOCUS 8 (UVR8) photoreceptors perceive UV-A/blue (315–500 nm) and UV-B (280–315 nm) radiation in plants, respectively. While the roles of CRYs and UVR8 have been studied in separate controlled-environment experiments, little is known about the interaction between these photoreceptors. Here, Arabidopsis wild-type L*er*, CRYs and UVR8 photoreceptor mutants (*uvr8-2*, *cry1cry2* and *cry1cry2uvr8-2*), and a flavonoid biosynthesis-defective mutant (*tt4*) were grown in a sun simulator. Plants were exposed to filtered radiation for 17 d or for 6 h, to study the effects of blue, UV-A, and UV-B radiation. Both CRYs and UVR8 independently enabled growth and survival of plants under solar levels of UV, while their joint absence was lethal under UV-B. CRYs mediated gene expression under blue light. UVR8 mediated gene expression under UV-B radiation, and in the absence of CRYs, also under UV-A. This negative regulation of UVR8-mediated gene expression by CRYs was also observed for UV-B. The accumulation of flavonoids was also consistent with this interaction between CRYs and UVR8. In conclusion, we provide evidence for an antagonistic interaction between CRYs and UVR8 and a role of UVR8 in UV-A perception.

Keywords: *Arabidopsis thaliana*, blue light, cryptochromes, flavonoids, photoreceptor interaction, solar radiation, sun simulator, transcript abundance, ultraviolet radiation, UVR8.

Introduction

Blue (400–500 nm), UV-A (315–400 nm), and UV-B (ground level UV-B, 290–315 nm) radiation are important components of sunlight that affect plant growth and development. Cryptochrome 1 and 2 (CRY1 and CRY2), Phototropin 1 and 2, and three LOV/F-box/Kelch-domain proteins (ZTL, FKF, and LKP2) are blue/UV-A photoreceptors (Lin, 2000; Christie *et al.*, 2015). Of these seven blue/UV-A photoreceptors, CRY1 and CRY2 are key regulators of photomorphogenic responses

such as inhibition of hypocotyl elongation and changes in gene expression in response to blue light (Yu *et al.*, 2010; Chaves *et al.*, 2011; Christie *et al.*, 2015). UV RESISTANCE LOCUS 8 (UVR8), the only UV-B photoreceptor reported in plants (Rizzini *et al.*, 2011), mediates photomorphogenesis in response to UV-B (Jenkins, 2017). Perception of UV-B and blue through UVR8 and CRYs, respectively, initiates signaling events that involve altered gene expression, which in turn affects photomorphogenesis of the whole plant (Liu *et al.*, 2011; Jenkins, 2017).

CONSTITUTIVELY PHOTOMORPHOGENIC 1 (COP1), an E3 ubiquitin ligase, is a central regulator of light signaling and photomorphogenesis in plants. COP1 interacts with CRY1 and UVR8 in a blue- and UV-B-dependent manner, respectively (Davis *et al.*, 2001; Favory *et al.*, 2009). The interactions of CRYs and UVR8 with COP1 stabilize the transcription factors ELONGATED HYPOCOTYL 5 (HY5) and HY5 HOMOLOG (HYH), both of which regulate the expression of most blue- and UV-responsive genes. Examples of genes induced by blue and UV-B that require CRYs and UVR8 include *CHALCONE SYNTHASE* (*CHS*), *CHALCONE ISOMERASE* (*CHI*), *DIHYDROFLAVONOL 4-REDUCTASE* (*DFR*), *EARLY LIGHT-INDUCED PROTEIN 2* (*ELIP2*) and *SOLANESYL DIPHOSPHATE SYNTHASE 1* (*SPS1*) (Brown *et al.*, 2005; Favory *et al.*, 2009; Yu *et al.*, 2010; OuYang *et al.*, 2015; Nawkar *et al.*, 2017).

One of the outcomes of the altered gene expression mediated by UVR8 in response to UV-B is a change in the concentrations of phenolic compounds (Kliebenstein *et al.*, 2002; Demkura and Ballaré, 2012; Morales *et al.*, 2013). Flavonoid glycosides and hydroxycinnamic acids (HCAs) are the two most important groups of phenolic compounds with UV-B-absorbing properties and their concentration is significantly increased upon exposure of plants to UV radiation (Tevini *et al.*, 1991; Burchard *et al.*, 2000). The first enzyme in the flavonoid biosynthesis pathway is CHS (Li *et al.*, 1993). The role of flavonoids in UV protection has been studied using *transparent testa 4* (*tt4*), which has a mutation in the *CHS* gene and is impaired in flavonoid biosynthesis (Li *et al.*, 1993). The accumulation of these compounds is known to be increased by UV radiation and blue light (Duell–Pfaff and Wellmann, 1982; Son and Oh, 2013). However, recent studies also showed that the induction of phenolic compounds was mainly driven by the blue component of sunlight in pea (Siipola *et al.*, 2015). In addition to UV and blue light, flavonoid biosynthesis is also modulated by other environmental factors including temperature (Bilger *et al.*, 2007; Pescheck and Bilger, 2019).

Despite recent advances in our understanding of plant responses regulated by CRYs and UVR8, there is still a significant gap in knowledge on how these photoreceptors together regulate responses to sunlight, a condition under which they both can be activated. It should also be noted that the absorption spectra of CRYs and UVR8 overlap. The CRYs absorption spectra extend from UV-B to green regions (Lin *et al.*, 1995; Ahmad *et al.*, 2002; Zeugner *et al.*, 2005; Banerjee *et al.*, 2007), while the UVR8 absorption spectrum extends from UV-C to the violet region (Daniel Farkas and Åke Strid, unpublished). This overlap in absorption spectra suggests the possibility of interaction between CRYs and UVR8. In fact, a crosstalk between UVR8 and other blue/UV-A photoreceptors has been previously suggested (Morales *et al.*, 2013). Both CRY and UVR8 signaling requires binding of the photoreceptors with COP1, and hence COP1 could mediate this interaction. UVR8 and CRYs mediate the expression of *HY5/HYH* which then induces the expression of some common downstream genes such as those involved in flavonoid biosynthesis (Ang *et al.*, 1998; Oravecz *et al.*, 2006; Lee *et al.*, 2007; Brown and Jenkins, 2008; Stracke *et al.*, 2010). In this way, *HY5/HYH* could also play a key role in mediating the interaction. Earlier experiments have elucidated the roles of CRYs or UVR8 in the perception of blue/UV-A and UV-B, respectively (Yu *et al.*, 2010; Rizzini *et al.*, 2011). However, no information exists on how these two photoreceptors together regulate plant growth, gene expression, and metabolite accumulation. In addition, most previous experiments have used artificial illumination with spectra very different from that of sunlight.

Another aspect that has been overlooked is the comparative study of blue-, UV-A-, and UV-B-mediated responses at short-term and long-term exposure, where short term would be from one to several hours and long term several days. Radiation-mediated responses including gene expression and phenolics biosynthesis can start within a few minutes to a few hours (Jenkins, 2009; Morales *et al.*, 2013). However, accumulation depends on the turnover rate, which is slower for phenolics than for gene transcripts.

To address these gaps in knowledge, we performed two factorial experiments using Arabidopsis mutants and light-absorbing filters. In the first experiment in a sun simulator, we used three photoreceptor mutants with impaired function in CRYs, UVR8, or both. The plants were exposed to long-term (17 d) or short-term (6 h) exposure to simulated sunlight modified by five long-pass filters with different cut-off wavelengths in UV and blue regions. In addition, we used the *tt4* mutant to understand the role of phenolic compounds in photoprotection. In this first experiment, we aimed to elucidate how UVR8 and CRYs together regulate growth, the changes in transcript abundance and the concentration of phenolic secondary metabolites in plants exposed to simulated sunlight. In the second experiment in outdoor conditions, we used the same photoreceptor mutants and filter treatments to confirm the roles of UVR8 and CRYs in regulating plant growth and survival in sunlight.

Materials and methods

Plant material

The sun simulator experiment was conducted in a small sun simulator (SunSCREEN growth chamber, 1.2 m×1.2 m×0.4 m) at the Research Unit Environmental Simulation at Helmholtz Zentrum München, Neuherberg, Germany and the outdoor experiment in the field area of the Viikki campus of the University of Helsinki (60°13′N, 25°1′E). The Arabidopsis genotypes used in both experiments were wild-type Landsberg *erecta* (L*er*) and the three photoreceptor mutants *uvr8-2* (Brown *et al.*, 2005), *cry1cry2* (Mazzella *et al.*, 2001), and *cry1cry2uvr8-2*. This new triple photoreceptor mutant was obtained by

crossing *uvr8-2* and *cry1cry2*. F2 triple mutant plants were genotyped by PCR using derived cleaved amplified polymorphic sequence (dCAPS) markers designed to detect homozygous mutations for *cry1* (Neff and Chory, 1998) and *cry2* (Mazzella *et al.*, 2001). For *uvr8-2*, genomic DNA was amplified with 5′-AACGTGTTTGCTTGGGGTAG-3′ and 5′-GGCTTACCGTTTCATCAGGA-3′ primers and PCR products were resolved on 2.5% agarose gel after digestion with endonuclease restriction enzyme *Dde*I. After digestion, 270 and 210 bp fragments were observed in L*er* and 270, 163, and 50 bp fragments in *uvr8-2*. In addition, a mutant impaired in flavonoid biosynthesis, *tt4* (Li *et al.*, 1993), was used in the sun simulator experiment.

Growth conditions and treatments in the sun simulator experiment

The seeds were sown in black plastic pots (7 cm×7 cm, Götz, Bischweier, Germany) filled with a commercial propagation substrate (Floradur B Seed, Floragard, Oldenburg, Germany) mixed with 1/6 volume of quartz sand (Dorsilit No. 7, Ø 0.6–1.2 mm, Dorfner, Hirschau, Germany). After sowing the seeds, the pots were kept in a dark and cold room at 4 °C for 3 d. Subsequently, the pots were transferred to the sun simulator and after 7 d seedlings were thinned to four per pot. There were four replicates in time (rounds 1–4). At each round, we collected one sample per treatment and genotype that consisted of 12 pooled rosettes from three independent pots. For L*er*, *uvr8-2*, and *cry1cry2* we had four replicates in all analyses (rounds 1–4). For *cry1cry2uvr8-2* and *tt4*, only two replicates were available (rounds 3 and 4, and rounds 1 and 2, respectively). This was because the triple mutant was not available until round 3. However, this limitation has been taken into consideration while doing the statistical analysis.

In the sun simulator, a combination of four lamp types (metal halide lamps: Osram Powerstar HQI-TS 400W/D; quartz halogen lamps: Osram Haloline 500W; blue fluorescent tubes: Philips TL-D 36W/BLUE; and UV-B fluorescent tubes: Philips TL 40W/12) filtered with a layer of Pyran glass (thickness 6 mm, Schott, Mainz, Germany) were used to obtain a natural balance of simulated global radiation throughout the UV to infrared spectrum. The lamps of different types were connected in separately controlled groups allowing the simulation of the diurnal variation in solar irradiance (Döhring *et al.*, 1996; Thiel *et al.*, 1996). A comparison between the spectral irradiance of the sun simulator and an outdoor spectrum has been shown in Aphalo *et al.* (2012, fig. 2.22). The sun simulator was at 21 °C/19 °C (day/night) air temperature and 65%/80% relative humidity under a 10 h photoperiod. Each of the two temperature- and humidity-controlled cuvettes (0.55 m×0.90 m×0.27 m) in the chamber was subdivided into five separate compartments, each covered by one of the five different filters (Ibdah *et al.*, 2002; Götz *et al.*, 2010). Near ambient solar UV >290 nm was provided by WG305 glass filters (Schott, Mainz, Germany), exclusion of wavebands <315 nm was provided by WG320 glass filters (Schott), exclusion of <350 nm was provided by Plexiglas 0Z023 GT acrylic filters (Evonik, Germany), exclusion of <400 nm was provided by Makrolife clear polycarbonate (Arla Plast, Sweden), and exclusion of <500 nm was provided by Plexiglas 1C33 GT acrylic filters (Evonik). The transmittance of these 3 mm-thick filters was measured with a spectrophotometer (Biochrom 4060 UV/VIS, Pharmacia LKB Biochrom Ltd, Cambourne, UK) (Fig. 1A).

PAR+UV-A and UV-B irradiances were adjusted independently. PAR and UV-A were increased from darkness to 900 and 80 μmol m^{-2} s^{-1}, respectively in steps from the start of the photoperiod and decreased in symmetrical steps until its end (Table 1A, B). UV-B radiation was switched on 1 h later than PAR+UV-A and switched off 1 h earlier. It was also increased in steps to a maximum value, which was 3.4 μmol m^{-2} s^{-1} in the >290 nm treatment (Table 1A, B). The exposure treatments were applied for two different lengths of time: long-term for 17 d and short-term for 6 h. For the 17 d exposure, the five filters were placed side by side on top of one of the two cuvettes from the start of the experiment until sampling at the end. For the 6 h exposure, polycarbonate filter was used to exclude UV radiation (290–400 nm) from the start of the experiment until 6 h before sampling when it was replaced by the above

mentioned five filters. The spectral irradiance under the different filters was measured with a double monochromator spectrometer (Bentham, Reading, UK) at a wavelength resolution and wavelength steps of 1 nm in the UV range and 2 nm in the visible range. The integrated photon irradiances for different wavebands and steps are given in Table 1A, B.

Immediately before harvesting, photographs of rosettes were taken to estimate mean rosette area. The samples from the 6 h treatment were collected first followed by the 17 d treatment samples with filter treatments and genotypes in random order. The short-term-treatment samples were harvested between 6 h and 6 h 45 min into the photoperiod and the long-term-treatment ones between 6 h 50 min and 7 h and 40 min into the photoperiod. Each harvested sample was immediately frozen in liquid nitrogen and stored at −80 °C. The frozen rosette leaves were ground with mortar and pestle in liquid nitrogen, and the powdered samples were divided into two Eppendorf tubes for storage and later assessment of gene expression and composition and concentration of phenolic compounds.

Growth conditions and treatments in the outdoor experiment

The seeds of L*er*, *uvr8-2*, *cry1cry2*, and *cry1cry2uvr8-2* were sown on 19 August 2016 in black plastic pots (8 cm×8 cm) containing a 1:1 mixture of pre-fertilized and limed peat (Kekkilä Professional, Vantaa, Finland) and vermiculite (Agra Vermiculite, PULL Rhenen, Rhenen, Netherlands), and kept in darkness at 4 °C for 3 d. Plastic trays containing two pots per genotype were brought outdoors on 22 August under four types of filters (1 m×1 m), matching the five used in the sun simulators, except for the filter that cuts at 315 nm, which was not included. Near ambient solar UV >290 nm was provided by Plexiglas 2458 GT (Evonik), exclusion of <350 nm was provided by Plexiglas 0Z023 GT, exclusion of <400 nm was provided by Makrolife clear polycarbonate, and exclusion of <500 nm was provided by Plexiglas 1C33 GT. The filter treatments were randomly assigned within four replicate blocks. All the genotypes were randomly distributed under each filter. The filters were held by wooden sticks at a slight inclination for rainwater to drain. The filters were kept 10–15 cm above the top of the plants, at the south and north, respectively. The transmittance of the filters was measured with a spectrophotometer (model 8453, Hewlett Packard, now Agilent, Waldbronn, Germany) (Fig. 1B). The air temperature for the duration of the experiment ranged from 2.3 to 21 °C. We modeled the hourly ambient spectra for the whole duration of the experiment (Lindfors *et al.*, 2009). Supplementary Fig. S1 at *JXB* online shows the daily photon exposure of PAR, and the daily photon ratios UV-B:PAR, UV-A$_{sw}$:PAR, UV-A$_{lw}$:PAR, and blue:PAR throughout the duration of the experiment. The spectral irradiance under each filter was measured with a spectroradiometer to validate the simulation (Maya2000 Pro, Ocean Optics, Largo, FL, USA).

The emergence of seedlings started under all treatments on 26 August. Five days after emergence (dae) seedlings were thinned to five plants per pot. Pictures were taken under the filters 17, 20, 24, and 27 dae to measure the growth and survival of plants.

Rosette growth area measurement in both sun simulator and outdoor experiment

Photographs were taken directly from above the plants with a camera supported by a tripod (Nikon D7000 AF-S NIKKOR 16–85 mm 1:3.5–5.6G ED, DX objective in the sun simulator experiment, and Olympus E-M1 M Zuiko 25 mm 1:18 objective in the outdoor experiment). In the sun simulator experiment, each photograph of six pots included a black reference target (2 cm×2 cm) on a white background. Raw images were first adjusted to equal brightness using the target's white background. Projected rosette area was determined as described by Wang (2016), using Fiji ImageJ (Schindelin *et al.*, 2012). In the outdoor experiment, each photograph of four pots was analysed for the projected rosette area similarly to what was described above. In this experiment, the photographs were taken of the same plants sequentially and the rosette area data were analysed as repeated measurements. The survival percentage was calculated from the same photographs.
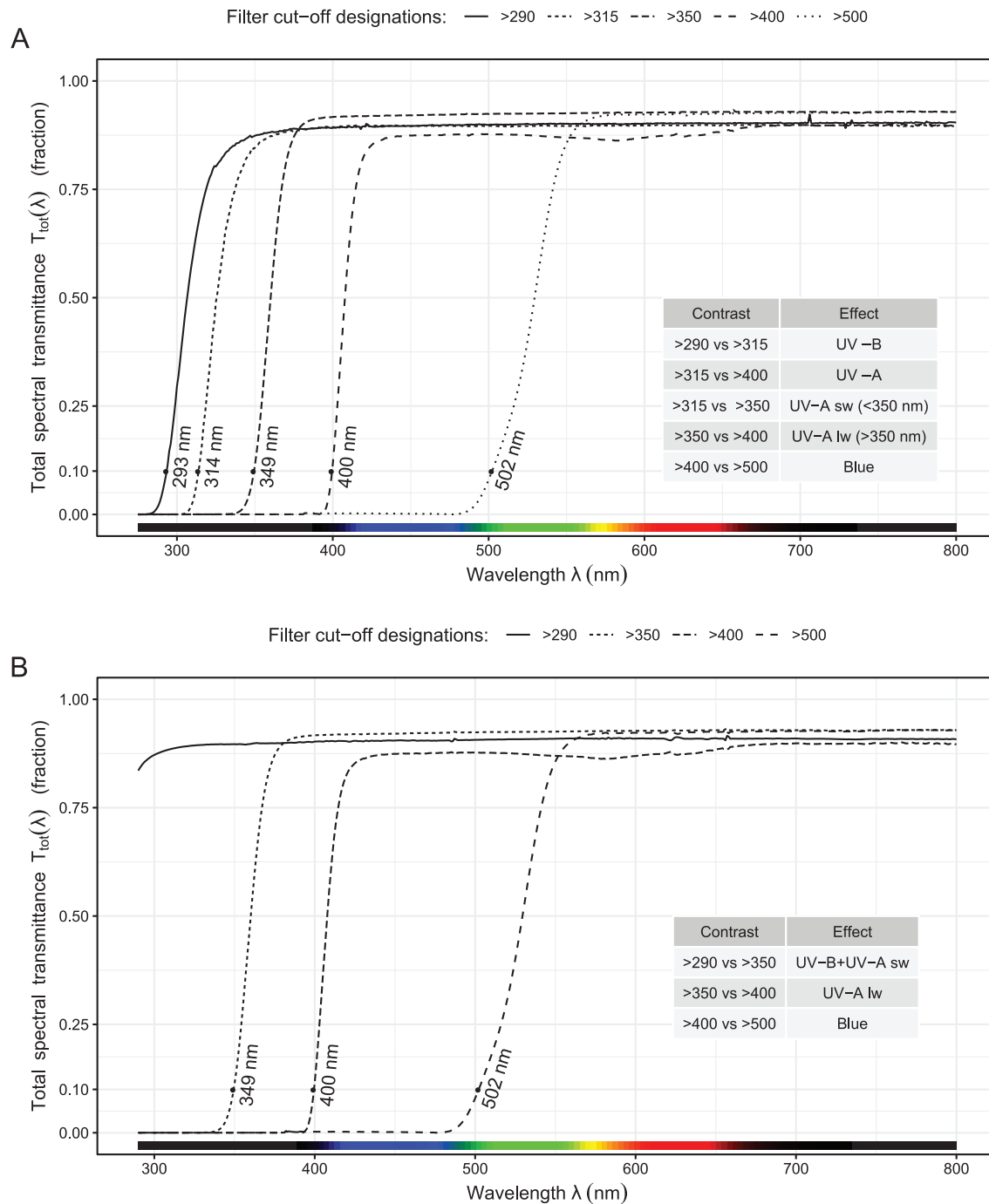
Fig. 1. Transmittance of filters used in (A) the sun simulator and (B) the outdoor experiment. See 'Materials and methods' for description of filters.

RNA extraction and quantitative real-time PCR in the sun simulator experiment

Total RNA was extracted from rosette leaves with a GeneJET Plant RNA Purification Kit according to manufacturer's guidelines (Thermo Fisher Scientific, Vilnius, Lithuania). RNA quantity and quality were checked using an ND-1000 Spectrophotometer (Thermo Fisher Scientific). Two micrograms of RNA from each sample were treated with DNase I (Thermo Fisher Scientific) in a 20 µl reaction mixture for 30 min at 37 °C. DNase I was inactivated by adding 2 µl EDTA to the reaction mixture and incubated for 10 min at 65 °C. This was then reverse-transcribed to cDNA using Revert Aid Reverse Transcriptase (Thermo Fisher Scientific), dNTP (Solis BioDyne, Tartu, Estonia) and oligo(dT) 20 primers (Sigma–Aldrich, St Louis, MO, USA) in 30 µl reaction mixture for 2 h at 50 °C. The cDNA was diluted to a final volume of 70 µl, and 1 µl was used as the template for PCR using 5× HOT FIREPol® EvaGreen® qPCR Mix Plus (Solis BioDyne) on a CFX 384 Real-Time PCR detection system (Bio-Rad, Hercules, CA, USA) in triplicate. PCR and data analysis were performed as in (Morales *et al.*, 2013). Information on the primers and three reference genes used in PCR is given in Supplementary Table S1.

Identification and quantification of phenolic compounds in the sun simulator experiment

Flavonoids were analysed according to Schmidt *et al.* (2010) with slight modification. Lyophilized, ground plant material (0.01 g) was extracted

Table 1. *Light treatments*

A. Treatment	PAR (µmol m^{-2} s^{-1})	Blue (µmol m^{-2} s^{-1})	UV-A (µmol m^{-2} s^{-1})	UV-B (µmol m^{-2} s^{-1})
>290 nm	920	220	80	3.4
>315 nm	910	220	75	0.3
>350 nm	890	210	40	<0.001
>400 nm	860	190	0.6	<0.001
>500 nm	620	1.0	<0.01	<0.001
B. Light step	**PAR (%)**	**Blue (%)**	**UV-A (%)**	**UV-B (%)**
LS 1	14	15	12	0.30
LS 2	45	45	48	46
LS 3	91	89	90	90
LS 4	100	100	100	100

(A) Photon irradiance at highest light level, step 4 (LS4). UV-B irradiance was calculated integrating from 290–315 nm, UV-A irradiance from 315–400 nm and blue irradiance from 400–500 nm. (B) Relative mean values at the different light steps. The photon irradiance at each light step for each treatment can be calculated by multiplying the values in (A) by those in (B), e.g. UV-A in treatment >350 nm at LS2 is 40×48/100=19.2 µmol m^{-2} s^{-1}.

with 600 µl of 60% aqueous methanol on a magnetic stirrer plate for 40 min at 20 °C. The extract was centrifuged at 19 000 *g* for 10 min at the same temperature, and the supernatant was collected in a reaction tube. This process was repeated twice with 300 µl of 60% aqueous methanol for 20 and 10 min, respectively; the three supernatants were combined. Next, the extract was evaporated until dry and then suspended in 200 µl of 10% aqueous methanol. The extract was centrifuged at 12 500 *g* for 5 min at 20 °C through a Corning® Costar® Spin-X® plastic centrifuge tube filter (Sigma–Aldrich) for the HPLC analysis. Each extraction was carried out in duplicate.

The concentration and composition of phenolics (flavonoid glycosides and HCAs) were determined from the filtrate using a series 1100 HPLC (Agilent Technologies, Waldbronn, Germany) equipped with a degaser, binary pump, autosampler, column oven, and photodiode array detector. An Ascentis® Express F5 column (150 mm×4.6 mm, 5 µm, Supelco, Bellefonte, PA, USA) was used to separate the compounds at a temperature of 25 °C. Eluent A was 0.5% acetic acid, and eluent B was 100% acetonitrile. The gradient used for eluent B was 5–12% (0–3 min), 12–25% (3–46 min), 25–90% (46–49.5 min), 90% isocratic (49.5–52 min), 90–5% (52–52.7 min), and 5% isocratic (52.7–59 min). The flow rate of 0.85 ml min^{-1} and wavelengths 280, 320, 330, 370 and 520 nm were used. The HCA and flavonoid derivatives were identified as deprotonated molecular ions and characteristic mass fragment ions according to Schmidt *et al*. (2010) and Neugart *et al*. (2015) by HPLC diode-array detection/electrospray ionization multi-stage mass spectrometry (HPLC-DAD/ESI-MS^n) using a Bruker amaZon SL ion trap mass spectrometer in negative ionization mode. Nitrogen was used as the dry gas (10 liters min^{-1}, 325 °C) and the nebulizer gas (40 psi) with a capillary voltage of −3500 V. Helium was used as the collision gas in the ion trap. The mass optimization for the ion optics of the mass spectrometer for quercetin was performed at *m/z* 301 or arbitrarily at *m/z* 1000. The MS^n experiments were performed in auto mode to MS^3 in a scan from *m/z* 200–2000. Standards (chlorogenic acid, quercetin 3-glucoside, kaempferol 3-glucoside, Roth, Karlsruhe, Germany) were used for external calibration curves in a semi-quantitative approach. Results are presented as mg g^{-1} dry weight (dw).

Statistical analysis

All statistical analyses were performed in R (R Core Team, 2018). Linear mixed-effect models with rounds, equivalent to blocks, as random-grouping factor were fitted using function lme from package 'nlme' (Pinheiro *et al*., 2018). Factorial ANOVA was used to assess the significance of the main effects treatment, genotype, and time (here time refers to 17 d and 6 h exposures) and of the interactions treatment×genotype, treatment×time, genotype×time for all variables measured. This analysis is shown in Supplementary Tables S2–S4. When ANOVA indicated

significant two-way interactions (*P*≤0.05), the function fit.contrast from the package gmodels (Warnes *et al*., 2018) was used to fit the contrasts of interests defined *a priori*. Thereafter, *P*-values from pairwise contrasts were adjusted with function p.adjust in R (Holm, 1979). The effect of blue light was tested from contrasts between the treatments >400 nm versus >500 nm, while the contrasts >315 nm versus >400 nm and >290 nm versus >315 nm allowed us to test specific UV-A and UV-B effects, respectively. We tested the effect of the short and long wavelength portions of UV-A (UV-A$_{sw}$ and UV-A$_{lw}$, respectively) by fitting contrasts for >315 nm versus >350 nm and >350 nm versus >400 nm (Fig. 1A).

Results

Growth and survival

Rosette area was measured to assess the roles of CRYs and UVR8 in maintaining growth of the plants in response to 17 d of blue, UV-A$_{lw}$, UV-A$_{sw}$, and UV-B wavebands in the sun simulator. The filter treatments had no detectable effect on the rosette area in L*er*, *uvr8-2*, and *tt4* (Fig. 2A, B). However, the rosette area of *cry1cry2* plants decreased in response to UV-A$_{lw}$ (*P*≤0.05), indicating a mediation by CRYs (Fig. 2B). Interestingly, *cry1cry2uvr8-2* showed a decreasing trend in the rosette area of plants in response to UV-A, UV-A$_{sw}$, and UV-A$_{lw}$ (Fig. 2B). The effect of UV-A as a whole was significant (*P*≤0.05) but not that of UV-A$_{lw}$ or UV-A$_{sw}$ individually. As most *cry1cry2uvr8-2* plants died in response to UV-B, the rosette area is not relevant here (Fig. 2A).

In addition to the quantitative differences, we found visible differences between genotypes and between filter treatments. In plants that did not receive either UV or blue radiation under the >500 nm filter, the margins of the leaves were curled downwards in all genotypes (Fig. 2A). This phenotype was not evident when plants were exposed to blue (Fig. 2A). In addition, *cry1cry2* had yellower leaves in response to blue and UV-A$_{lw}$ whereas *cry1cry2uvr8-2* had them in response to blue, UV-A$_{lw}$, and UV-A$_{sw}$. On the other hand, *uvr8-2* had some of its older leaves darker in response to UV-A$_{lw}$, UV-A$_{sw}$, and UV-B (Fig. 2A). This suggests that the photoreceptors played a role in the accumulation of various pigments in leaves under simulated sunlight.
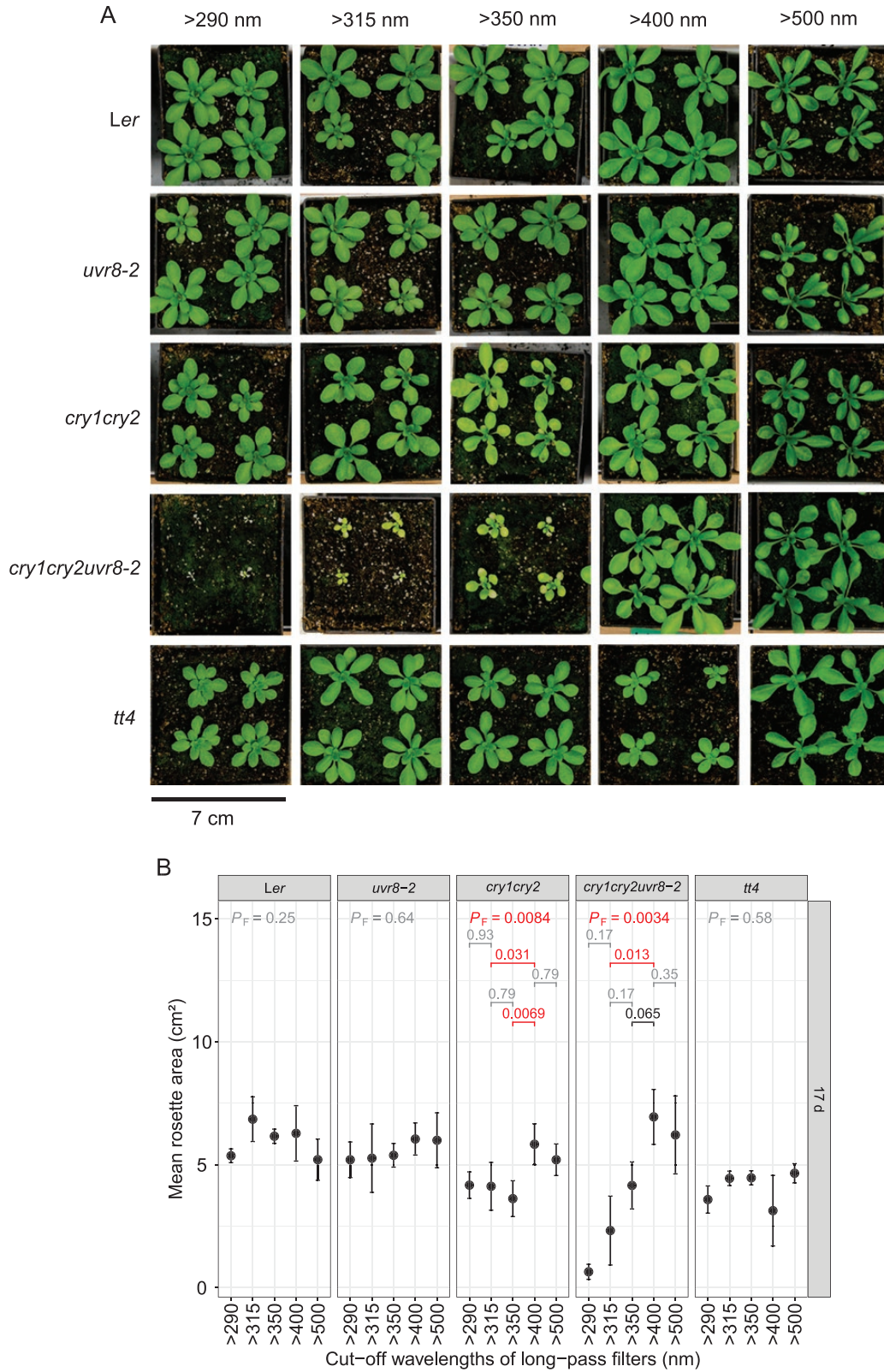
Fig. 2. Growth of the Arabidopsis plants in sun simulator experiment. (A) Photographs of plants after 17 d of treatment showing morphology and survival. A representative pot from each genotype and treatment is shown. (B) Rosette area of all the plants after 17 d of treatment. Mean ±1 SE.

The role of CRYs and UVR8 in the regulation of growth and survival was further examined in the outdoor experiment. Here, the rosette area was similar for L*er*, *uvr8-2*, and *cry1cry2* (Fig. 3A, B). However, *cry1cry2uvr8-2* plants failed to grow when exposed to solar UV-B+UV-A$_{sw}$ and survived in only a few pots when exposed to solar UV-A$_{lw}$ (Fig. 3A–C). Here it should be noted that in the outdoor experiment, a small fraction of ambient diffuse UV-B and
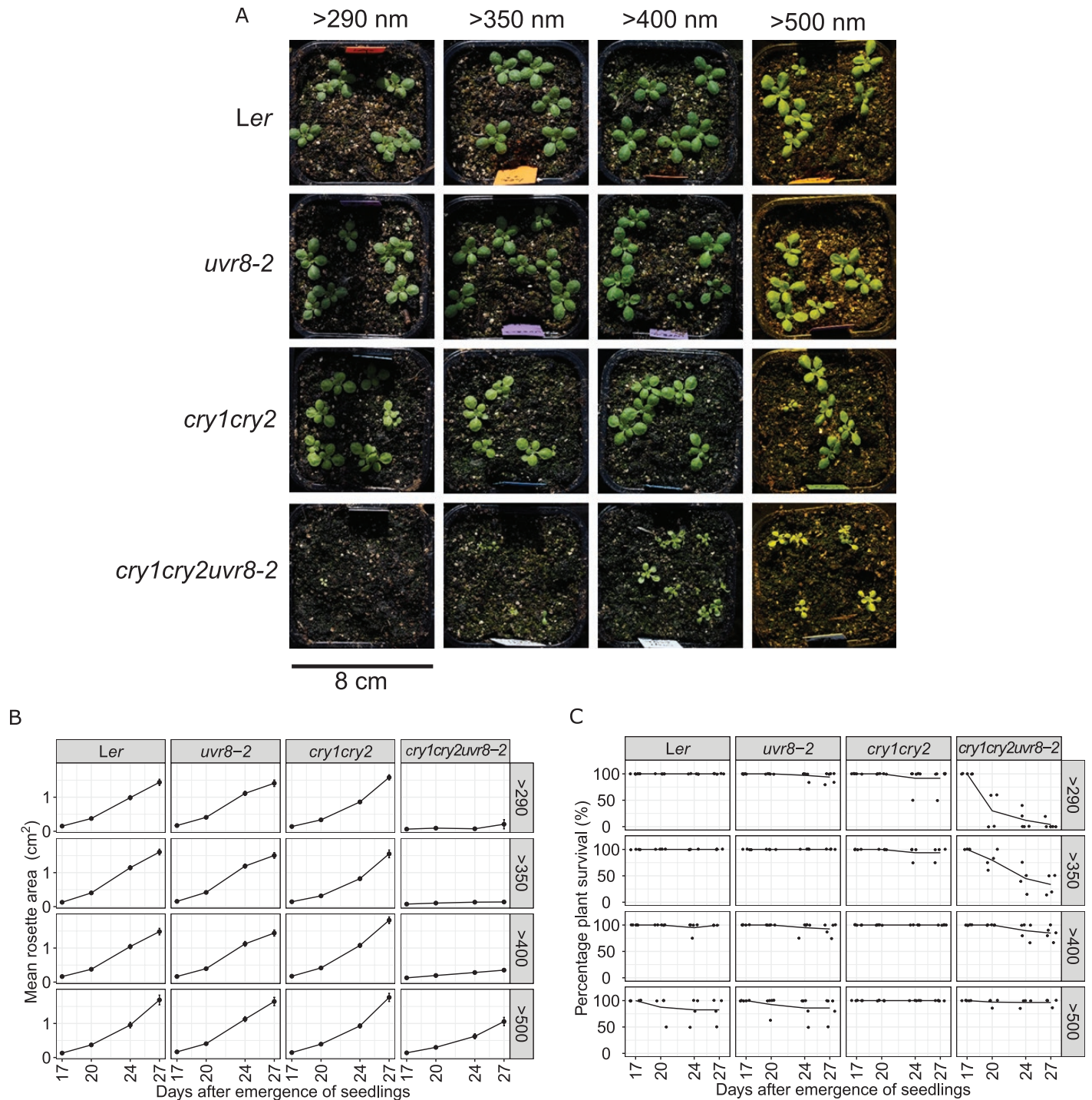
Fig. 3. Growth of the Arabidopsis plants in outdoor experiment. (A) Photographs of plants after 24 d of treatment. A representative pot from each genotype and treatment is shown. A strong color cast is present in the photographs taken under the >500 nm filter, which is yellow in color. (B) Time course of rosette area between 17 and 27 d of treatment. Mean ±1 SE. (C) Time course of plant survival between 17 and 27 d of treatment. Data points are the overall mean and means for individual biological replicates.

UV-A reached the plants even under filters fully blocking these wavebands.

Under full spectrum sunlight (>290 nm) only 4% of the *cry1cry2uvr8-2* plants survived at the end of the experiment (Fig. 3C). The survival percentage was 30% when UV-B+UV-A$_{sw}$ were attenuated from sunlight (>350 nm). The survival improved to more than 80% when *cry1cry2uvr8-2* did not receive UV-B+UV-A$_{sw}$ and UV-A$_{lw}$. Furthermore, almost all *cry1cry2uvr8-2* plants survived when they did not receive UV-B+UV-A$_{sw}$, UV-A$_{lw}$, and blue (>500 nm). The mean survival percentage of plants of the other three genotypes was 80% or more under all treatments (Fig. 3C).

Transcript abundance

We measured changes in transcript abundance of nine UV- and blue light-responsive marker genes after 17 d and 6 h of exposure to filter treatments. Out of these nine genes, *HY5* and

REPRESSOR OF UV-B PHOTOMORPHOGENESIS 2 (*RUP2*) are involved in UVR8 and/or CRY signaling; *CHS* (*TT4*), *CHI* (*TT5*), *DFR*, *FLAVONOID 3′-HYDROXYLASE* (*F3′H* or *TT7*, Schoenbohm *et al.*, 2000), and *PRODUCTION OF ANTHOCYANIN PIGMENT 1* (*PAP1*) are involved in biosynthesis of flavonoids and anthocyanins; *SPS1* is involved in ubiquinone biosynthesis; and *ELIP2* is involved in multiple light signaling pathways. Seven genes (*CHS*, *CHI*, *ELIP2*, *F3′H*, *HY5*, *RUP2*, and *SPS1*) showed significant induction to more than one treatment–genotype–time combination ($P \leq 0.05$, Fig. 4A–G) that could be mediated by CRYs or UVR8. On the other hand, two genes (*DFR* and *PAP1*) did not respond significantly to any combination that could be assigned to these photoreceptors (see Supplementary Fig. S2). Furthermore, most responses in transcript abundance for these seven genes were observed after 6 h of treatments, and only a few after 17 d (Fig. 4A–G).

The transcript abundance of *CHS*, *HY5*, *RUP2*, and *SPS1* increased in response to 6 h of blue in L*er* and *uvr8-2* ($P \leq 0.05$) but not in *cry1cry2*, indicating a mediation by CRYs (Fig. 4A, E–G). On the other hand, *RUP2* increased in response to 6 h of UV–B in L*er* and *cry1cry2* ($P \leq 0.05$) but not in *uvr8-2*, indicating a mediation by UVR8 (Fig. 4F).

The transcript abundance of *CHI* increased in response to 6 h of UV–A in L*er* alone ($P \leq 0.05$), apparently mediated by both UVR8 and CRYs (Fig. 4B). The absence of CRYs resulted in increased transcript levels of *CHS*, *ELIP2*, *RUP2*, and *SPS1* in response to 6 h of UV–A$_{sw}$ in *cry1cry2* (Fig. 4A, C, F, G). This induction of transcripts was only significant in *cry1cry2* and not in L*er*, *uvr8-2*, or *cry1cry1uvr8-2*. This indicates that CRYs negatively regulated the UVR8-mediated gene expression in response to UV–A$_{sw}$, in the presence of UV–A$_{lw}$ and PAR.

Similarly, an absence of CRYs led to enhanced levels of *CHS*, *F3′H*, and *SPS1* in response to 6 h of UV–B in *cry1cry2* ($P \leq 0.05$), and this enhancement was not detected as significant in L*er* (Fig. 4A, D, G). The transcript levels of *ELIP2* and *RUP2* were also enhanced to a higher magnitude by 6 h of UV–B in *cry1cry2* than in L*er* (Fig. 4C, F). Furthermore, *cry1cry2uvr8-2* was impaired in these responses. These observations indicate that CRYs also negatively regulated the UVR8-mediated gene expression in response to UV–B in the presence of UV–A$_{sw}$, UV–A$_{lw}$, and PAR.

The response of transcript abundance to 17 d treatments was mostly non–significant ($P > 0.05$). The few exceptions included an induction of *ELIP2* in L*er* and *uvr8-2* in response to blue light, which indicates a mediation by CRYs (Fig. 4C). The induction of *RUP2* in response to 17 d of blue treatment was only detected significantly in L*er* (Fig. 4F) while the absence of CRYs resulted in the induction of *CHS* in response to 17 d of UV–A$_{sw}$ in *cry1cry2* (Fig. 4A).

The *tt4* mutant showed similar patterns of gene expression response to L*er* to 6 h and 17 d of treatments, but only in very few cases were these responses detected as significant, probably because of fewer replicates (Fig. 4A–G).

Phenolic compound accumulation

We identified 11 phenolic compounds that included four kaempferol derivatives, three quercetin derivatives, and four HCAs. The kaempferol derivatives were kaempferol-3-*O*-rutinoside-7-*O*-rhamnoside (K-3-rut-7-rha), kaempferol-3-*O*-diglucoside-7-*O*-rhamnoside (K-3-diglc-7-rha), kaempferol-3-*O*-glucoside-7-*O*-rhamnoside (K-3-glc-7-rha), and kaempferol-3-*O*-rhamnoside-7-*O*-rhamnoside (K-3-rha-7-rha) (Fig. 5A–E). The quercetin derivatives were: quercetin-3-*O*-rutinoside-7-*O*-rhamnoside (Q-3-rut-7-rha), quercetin-3-*O*-diglucoside-7-*O*-rhamnoside (Q-3-diglc-7-rha), and quercetin-3-*O*-rhamnoside-7-*O*-rhamnoside (Q-3-rha-7-rha) (Fig. 6A–D). The HCAs included hydroxyferuloyl glucoside (HFG), hydroxyferuloyl malate (HFM), sinapoyl malate (SM), and an unknown acid (Fig. 7A–E). The sum of the derivatives in each group was used to quantify total kaempferols (Fig. 5A), total quercetins (Fig. 6A), and total HCAs (Fig. 7A).

We found an increase in the concentration of total kaempferols in L*er* and *cry1cry2* ($P \leq 0.05$) but not in *uvr8-2* after 17 d of UV–B, which indicates mediation by UVR8. However, no clear photoreceptor-mediated response was detected after 6 h (Fig. 5A). Assessment of individual kaempferol derivatives showed an increase in the concentration of three out of four kaempferol derivatives (K-3-rut-7-rha, K-3-glc-7-rha, and K-3-rha-7-rha) in L*er* and *cry1cry2* after17 d of UV–B ($P \leq 0.05$, Fig. 5B, D, E).

In comparison to the kaempferols, the total quercetins accumulated in lower amounts (<50% than the total kaempferols under filter >290 nm, cf. Figs 5A, 6A). After 6 h, the concentration of total quercetins increased in response to UV–A$_{lw}$ in L*er*, *uvr8-2*, and *cry1cry2uvr8-2* ($P \leq 0.05$), suggesting mediation by photoreceptors other than CRYs and UVR8 (Fig. 6A). We also observed an increased concentration of total quercetins in response to 6 h of UV–B in L*er* ($P = 0.053$) and *cry1cry2* ($P \leq 0.05$), suggesting a mediation by UVR8. After 17 d, the concentration of total quercetins increased in response to UV–B in L*er* ($P \leq 0.05$). However, this response could not be assigned to UVR8 due to high variation in *cry1cry2* ($P = 0.085$, Fig. 6A). The analysis of individual quercetin derivatives showed that all three quercetins (Q-3-rut-7-rha, Q-3-diglc-7-rha, and Q-3-rha-7-rha) also responded in a similar way as the total quercetins. In addition, Q-3-diglc-7-rha and Q-3-rha-7-rha concentration increased significantly in *cry1cry2* ($P \leq 0.05$) in response to 6 h of UV–B, also suggesting mediation by UVR8 (Fig. 6C, D).

Unlike kaempferols and quercetins, the changes in the concentration of HCAs were less pronounced and could not be assigned to UVR8 or CRYs (Fig. 7A–E). Of the four HCAs, SM was present in highest concentration in all treatments and genotypes at 6 h and 17 d (Fig. 7A, D).

We did not detect kaempferol derivatives in the *tt4* mutant at any time point, as expected from a mutant defective in flavonoid biosynthesis (Fig. 5A–E). The quercetin derivatives also accumulated to a very low concentration (<0.15 mg g^{-1} dry weight) or were not detected in *tt4* (Fig. 6A–D). HCAs were present in both L*er* and *tt4* and after both 6 h and 17 d treatments (Fig. 7A–E). HFG and HFM accumulated to a higher concentration in *tt4* than in L*er*, after both 6 h and 17 d in all the treatments (Fig. 7B, C).
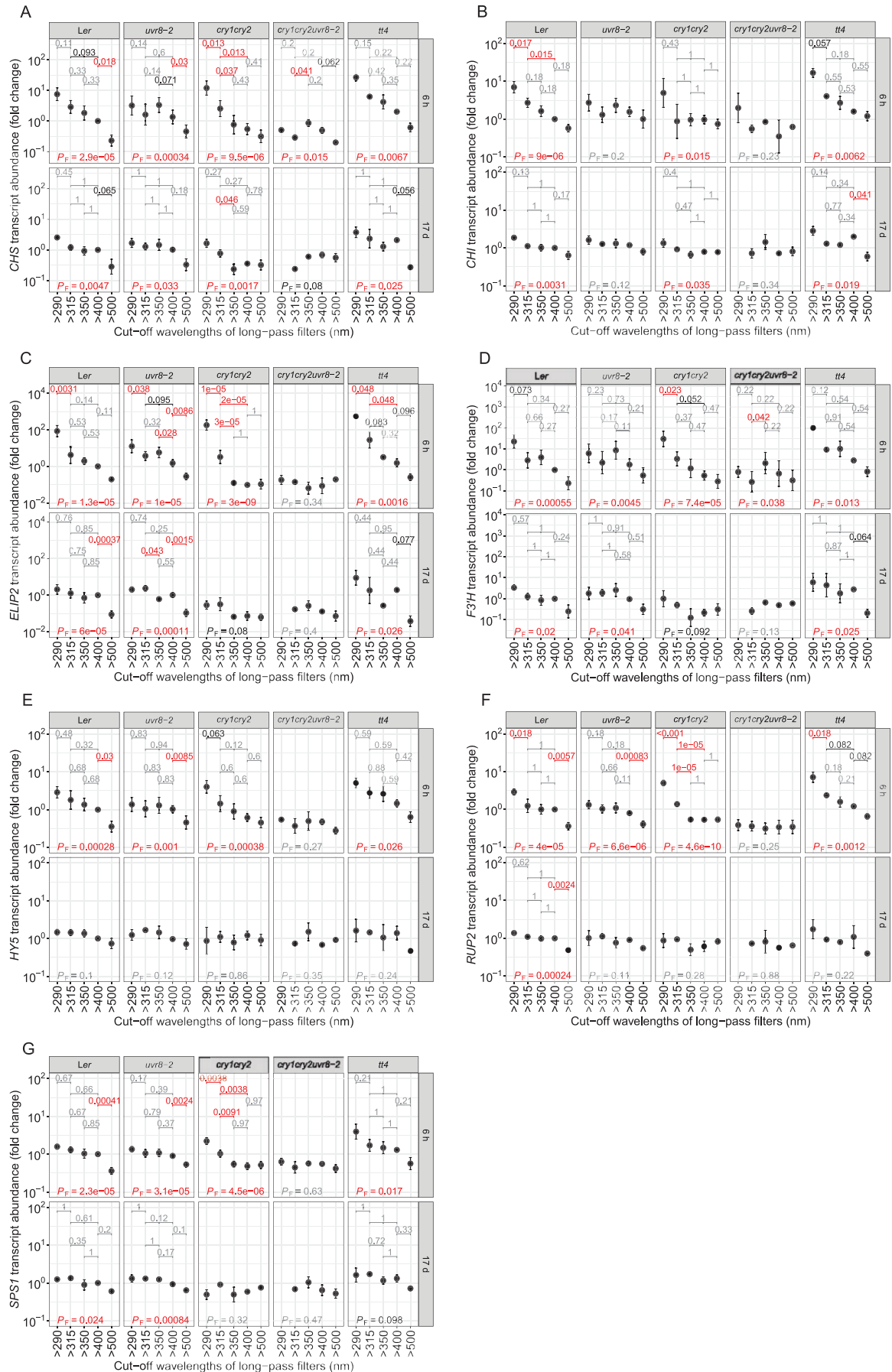
Fig. 4. Transcript abundance of seven marker genes in leaves of Arabidopsis plants after 6 h (upper row) or 17 d (lower row) of treatment. (A) *CHS*, (B) *CHI*, (C) *ELIP2*, (D) *F3′H*, (E) *HY5*, (F) *RUP2*, and (G) *SPS1*. Mean ±1 SE. The horizontal bars represent pair-wise comparisons between treatments within each genotype. The P_F value (at the bottom of each panel) is from a one-way ANOVA testing the overall effect of filter treatments within each genotype.
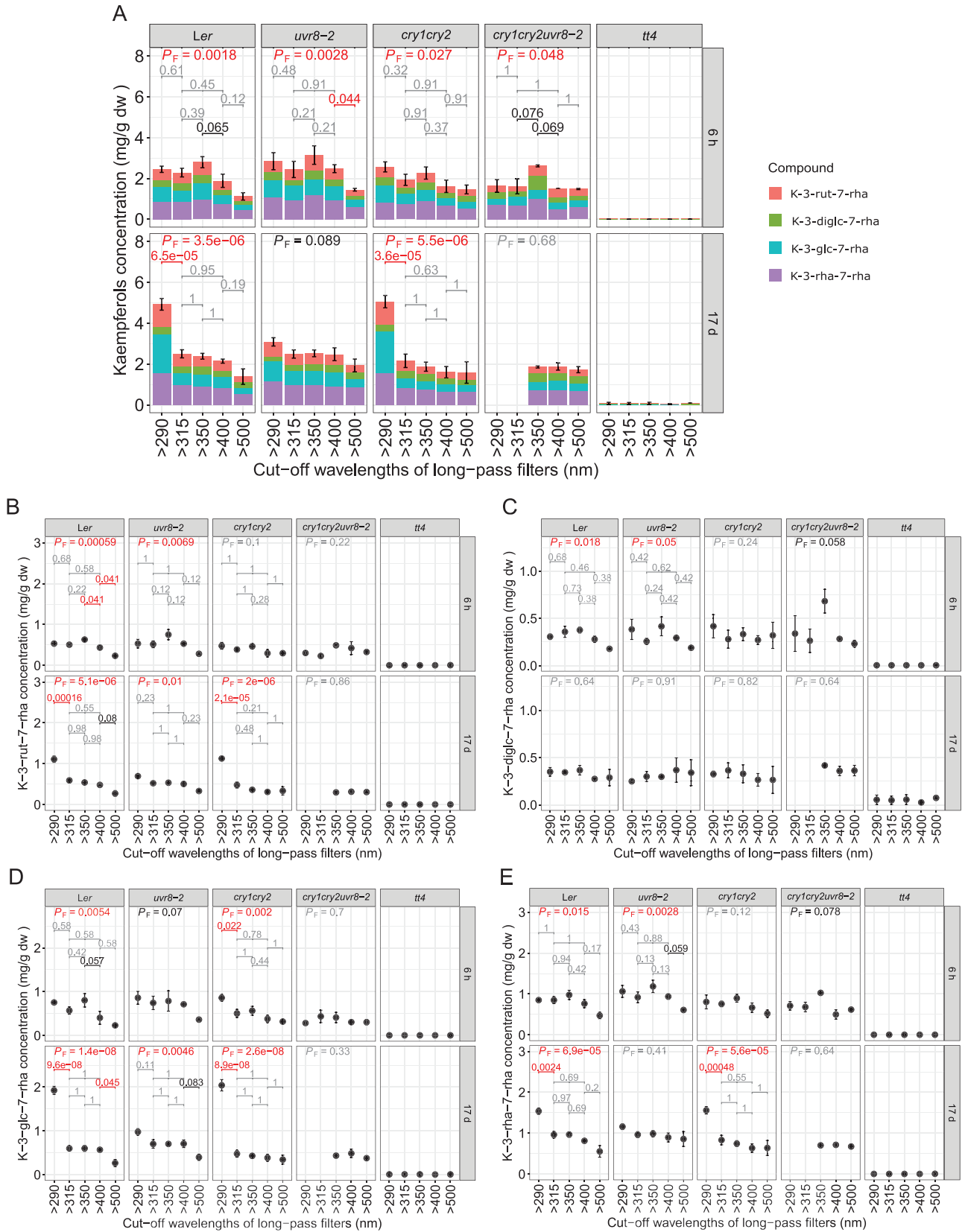
Fig. 5. Kaempferols in leaves of Arabidopsis plants after 6 h (upper row) and 17 d (lower row). (A) Stacked bars showing total concentration and composition. (B–E) Concentration of individual kaempferol derivatives: (B) K-3-rut-7-rha, (C) K-3-diglc-7-rha, (D) K-3-glc-7-rha, and (E) K-3-rha-7-rha. Mean ±1 SE. The horizontal bars represent pair-wise comparisons between treatments within each genotype. The P_F value (at the top of each panel) is from a one-way ANOVA testing the overall effect of filter treatments within each genotype. K-3-diglc-7-rha co-eluted with Q-3-glc-7-rha, but K-3-diglc-7-rha was the major compound. Therefore, K-3-diglc-7-rha concentration represents a very small amount of Q-3-glc-7-rha concentration too, which could not be quantified separately.

Fig. 6. Quercetins in leaves of Arabidopsis plants after 6 h (upper row) and 17 d (lower row). (A) Stacked bars showing total concentration and composition. (B–D) Concentration of individual quercetin derivatives: (B) Q-3-rut-7-rha, (C) Q-3-diglc-7-rha, and (D) Q-3-rha-7-rha. Mean ±1 SE. The horizontal bars represent pair-wise comparisons between treatments within each genotype. The P_F value (at the top of each panel) is from a one-way ANOVA testing the overall effect of filter treatments within each genotype.

Fig. 7. Hydroxycinnamic acids in leaves of Arabidopsis plants after 6 h (upper row) and 17 d (lower row). (A) Stacked bars showing total concentration and composition. (B–E) Concentration of individual hydroxycinnamic acid derivatives: (B) hydroxyferuloyl glucoside, (C) hydroxyferuloyl malate, (D) sinapoyl malate, and (E) unknown compound. Mean ±1 SE. The horizontal bars represent pair-wise comparisons between treatments within each genotype. The P_F value (at the top of each panel) is from a one-way ANOVA testing the overall effect of filter treatments within each genotype.

Discussion

The simultaneous absence of both CRYs and UVR8 was detrimental for plants exposed to UV-A and UV-B

The role of CRYs and UVR8 in Arabidopsis plants' growth and survival has been shown earlier using *cry1cry2* and *uvr8* mutants (Brown *et al.*, 2005; Mao *et al.*, 2005; Favory *et al.*, 2009; Morales *et al.*, 2013), but not studied in *cry1cry2uvr8-2* as reported here. It is known that the absence of CRYs is not lethal for Arabidopsis plants growing in the presence of blue light (Mao *et al.*, 2005). Similarly, an absence of functional UVR8 is also not lethal for plants growing in sunlight containing UV-B (Morales *et al.*, 2013). Morales *et al.* (2013) suggested that other pathways independent of UVR8 signaling might play a role in plant survival under UV-B exposure. Our results showing that *cry1cry2* and *uvr8-2* plants survived under full-spectrum simulated and natural sunlight agree with these previous findings (Figs 2, 3). Morales *et al.* (2013) also showed a reduced growth in *uvr8-2* under sunlight containing UV-A and UV-B, whereas Favory *et al.* (2009) reported visible leaf curling, cell death, and smaller *uvr8-7* plants when exposed to 27 d of simulated sunlight containing UV-B. However, under our conditions, using step increases and decreases in irradiance, we did not detect any significant difference between the rosette area of L*er* and *uvr8-2* across all treatments (Fig. 2A, B). We also did not observe any visible leaf curling or necrotic lesions in *uvr8-2* plants under UV-B or UV-A (Fig. 2A).

A possible explanation for the different results from those of Favory *et al.* (2009), even though both experiments were conducted in the same sun simulator, could be the duration of the experiment until observations were made (in our case 17 d, Favory *et al.* 27 d). However, a more likely reason could be the difference between the daily protocols used for UV-B and PAR irradiation. Favory *et al.* (2009) used 14 h of PAR (40 mol m^{-2} d^{-1}) and 12 h of UV-B (151 mmol m^{-2} d^{-1}), whereas we used 10 h of PAR (22 mol m^{-2} d^{-1}, except under blue attenuation where it was 15 mol m^{-2} d^{-1}) and 8 h of UV-B (82 mmol m^{-2} d^{-1}). The daily totals used in both experiments were very different but the maximum irradiances were similar (PAR: 800 µmol m^{-2} s^{-1}, UV-B: 3.5 µmol m^{-2} s^{-1} in Favory *et al.*'s experiment and PAR: 900 µmol m^{-2} s^{-1}, UV-B: 3.4 µmol m^{-2} s^{-1} in our experiment), as a result of stepwise increase and decrease in irradiance and shorter day length in our experiment. In particular, the stepwise increase and decrease in UV-B ensured that a longer time is available for plants to trigger CRY-dependent protective responses and photoreactivation of DNA damage. Our data also highlight the importance of CRY signaling in the maintenance of normal growth in the presence of UV-A$_{lw}$.

The most interesting observation was that the plants lacking both functional CRYs and UVR8 did not survive under either natural or simulated sunlight containing UV-B (Figs 2, 3). This consistent evidence from both sun simulator and outdoor experiments indicates a key role of CRYs in plant growth and survival under UV-B, which can explain the survival of *uvr8-2* plants in our experiments. With this work, we demonstrate a role of CRYs in growth and survival under UV-B and UV-A, and a role of UVR8 in growth and survival under UV-A, which have not been previously reported.

Interaction between CRYs and UVR8 under UV-A and UV-B

Most of the changes in transcript abundance dependent on CRYs and UVR8 were observed after 6 h of treatments (Fig. 4). This was expected since several marker genes used in our experiment (*CHS*, *F3′H*, *HY5*, *RUP2*, and *SPS1*) are known to be regulated early in response to light (Morales *et al.*, 2013).

Fuglevand *et al.* (1996) and Liu *et al.* (2018) showed that CRY1 mediated the induction of *CHS* in response to blue light in Arabidopsis and tomato, respectively, whereas Gruber *et al.* (2010) showed *RUP2* induction in response to blue light. Furthermore, CRYs are well known to induce *HY5* in response to blue light. Our results showed that CRYs mediated the induction of *CHS*, *HY5*, and *RUP2* in response to 6 h of blue light, which agreed with these previous findings (Fig. 4A, E, F).

In our experiment, UVR8 mediated the induction of *RUP2* in response to 6 h of UV-B in agreement with Gruber *et al.* (2010). However, the expected and previously reported UVR8-mediated induction of *CHS*, *F3′H*, and *SPS1* in response to UV-B (Ulm *et al.*, 2004; Morales *et al.*, 2013) were not observed in our experiment (Fig. 4A, D, G). Interestingly, the absence of CRYs enabled the induction of these genes under 6 h of UV-B, which suggests an antagonistic interaction between CRY and UVR8 signaling. We propose that this antagonistic interaction is the result of competition between the two photoreceptors for COP1 binding. The interaction could be due to a higher affinity between COP1 and CRYs than between COP1 and UVR8 in simulated sunlight. Evidence exists that the interaction of UVR8 with COP1 under extended UV-B exposure might depend on removal of COP1 from CRY signaling pathways (Favory *et al.*, 2009). This does not preclude preferential binding of COP1 to CRYs during short-term exposure as in our 6 h treatment.

The involvement of both CRYs and UVR8 in the perception of UV-A has been previously proposed (Wade *et al.*, 2001; Morales *et al.*, 2013; Brelsford *et al.*, 2018). Here, we show that both CRYs and UVR8 are simultaneously required for transcript accumulation of *CHI* under UV-A (Fig. 4B). This indicates an interaction between UVR8 and CRY signaling in the UV-A region.

In addition, contrary to what might be expected from a mutant lacking CRYs, *cry1cry2* showed induction of *CHS*, *ELIP2*, *RUP2*, and *SPS1* in response to UV-A, especially in UV-A$_{sw}$ (Fig 4A, C, F, G). This increased expression is mediated by UVR8, given the missing response in *cry1cry2uvr8-2*. This demonstrates a novel role of UVR8 in the regulation of transcript abundance under UV-A when functional CRYs are absent. Moreover, L*er* lacked these responses. Hence, we conclude that CRYs were suppressing the UVR8-mediated gene expression under UV-A$_{sw}$ in L*er*.

UVR8 mediated the accumulation of flavonoids under UV-B

We observed a UVR8-mediated increase in the concentration of kaempferols after 17 d of UV-B exposure (Fig. 5A, B, D, E). This was in overall agreement with earlier studies on the role of UVR8 in the induction of phenylpropanoid metabolism and flavonoid accumulation (Kliebenstein *et al.*, 2002;

Favory *et al.*, 2009; Gruber *et al.*, 2010; Morales *et al.*, 2013). UVR8 may have also mediated the increased concentration of quercetins after 17 d of UV–B exposure, but this could not be confirmed due to high variation in *cry1cry2* (Fig. 6A–D).

The concentration of both total kaempferols and quercetins and their individual derivatives responded to treatments. These results partially agree with experiments done in sunlight with birch seedlings (Morales *et al.*, 2010), Arabidopsis plants (Morales *et al.*, 2013), and pea plants (Siipola *et al.*, 2015) where it was shown that only the concentration of individual derivatives, and not the total, responded to the treatments. The increased accumulation of total kaempferols in response to 17 d of UV–B mediated by UVR8 is explained by the individual responses of three out of four kaempferol derivatives (Fig. 5A, B, D, E). Three quercetin derivatives also responded similarly to the total quercetins (Fig. 6A–D). In addition, 6 h of UV–B increased the concentration of K–3–glc–7–rha, Q–3–diglc–7–rha, and Q–3–rha–7–rha only in *cry1cry2*, dependent on UVR8, which agrees with the induction of *CHS* in response to 6 h of UV–B in the same photoreceptor mutant (Figs 5D, 6C, 6D, 4A). This links the antagonistic interaction between the two photoreceptors in the regulation of transcript abundance to secondary metabolite accumulation.

The HCAs were mostly constitutively present in L*er* and all the photoreceptor mutants, irrespective of treatment and time (except for *cry1cry2uvr8-2* where samples were missing for treatments with lethal effect on plants) (Fig. 7A–E). The same was true for SM, which was present in the highest concentration among all HCAs (Fig. 7D). SM is known to provide UV–B screening (Li *et al.*, 1993; Baker *et al.*, 2016). However, we could not detect any change in the concentration of SM in response to UV–B in any genotype. This suggests that SM provides protection against UV in sunlight, independent of perception of blue and UV–B by CRYs and UVR8.

The TT4 mutation was not detrimental for plants growing in simulated sunlight

The rosette area of *tt4* was not affected by any treatments after 17 d (Fig. 2A, B). Furthermore, visually we did not observe any damage, discoloration, or necrotic lesions in any *tt4* plants despite the lack of most of the flavonoid compounds (Fig. 2A). This agrees with Li *et al.* (1993) where daily UV–B exposure (8 kJ day^{-1}) did not have any drastic effect on the size and morphology of *tt4* plants. They explained the lack of UV–B sensitivity in the *tt4* mutant as due to the higher accumulation of sinapate esters (30–50% more) in response to UV–B, when compared with L*er*. However, in our experiment, HFG and HFM could also play a role in UV–B protection, in addition to SM in *tt4*. Furthermore, the protective role of these compounds may extend from UV–B to blue regions of simulated sunlight.

Conclusions

Both CRYs and UVR8 independently enabled growth and survival of plants under solar levels of UV, while their joint absence was lethal under UV–B. UVR8 mediated the increase in the concentration of flavonoids under UV–B. For gene expression, CRYs played a major role under blue light and UVR8 under UV–B radiation while both CRYs and UVR8 jointly mediated responses to UV–A. We provide evidence for an antagonistic interaction between CRYs and UVR8, which could be possibly mediated by COP1. However, further experiments are required for the elucidation of the mechanisms of interaction between CRYs and UVR8.

Supplementary data

Supplementary data are available at *JXB* online.

Fig. S1. Simulated daily total of PAR, and the daily photon ratios UV–B:PAR, UV–A$_{sw}$:PAR, UV–A$_{lw}$:PAR, and blue:PAR.

Fig. S2. Transcript abundance of two genes (*DFR* and *PAP1*).

Table S1. Information on primers used in qRT-PCR.

Table S2. Summary of the ANOVA from growth and survival analysis.

Table S3. Summary of the ANOVA from qRT-PCR analysis.

Table S4. Summary of the ANOVA from phenolic compounds analysis.

References

Ahmad M, Grancher N, Heil M, Black RC, Giovani B, Galland P, Lardemer D. 2002. Action spectrum for cryptochrome-dependent hypocotyl growth inhibition in Arabidopsis. Plant Physiology **129**, 774–785.

Ang LH, Chattopadhyay S, Wei N, Oyama T, Okada K, Batschauer A, Deng XW. 1998. Molecular interaction between COP1 and HY5 defines a regulatory switch for light control of *Arabidopsis* development. Molecular Cell **1**, 213–222.

Aphalo PJ, Albert A, Björn LO, Mc Leod A, Robson TM, Rosenqvist E (eds.). 2012. Beyond the visible: a handbook of best practice in plant UV photobiology. COST Action FA0906 *UV4growth*. Helsinki: University of Helsinki, Division of Plant Biology.

Baker LA, Horbury MD, Greenough SE, Allais F, Walsh PS, Habershon S, Stavros VG. 2016. Ultrafast photoprotecting sunscreens in natural plants. The Journal of Physical Chemistry Letters **7**, 56–61.

Banerjee R, Schleicher E, Meier S, Viana RM, Pokorny R, Ahmad M, Bittl R, Batschauer A. 2007. The signaling state of *Arabidopsis* cryptochrome 2 contains flavin semiquinone. The Journal of Biological Chemistry **282**, 14916–14922.

Bilger W, Rolland M, Nybakken L. 2007. UV screening in higher plants induced by low temperature in the absence of UV-B radiation. Photochemical & Photobiological Sciences **6**, 190–195.

Brelsford CC, Morales LO, Nezval J, Kotilainen TK, Hartikainen SM, Aphalo PJ, Robson TM. 2018. Do UV-A radiation and blue light during growth prime leaves to cope with acute high light in photoreceptor mutants of Arabidopsis thaliana? Physiologia Plantarum **165**, 537–554.

Brown BA, Cloix C, Jiang GH, Kaiserli E, Herzyk P, Kliebenstein DJ, Jenkins GI. 2005. A UV-B-specific signaling component orchestrates plant UV protection. Proceedings of the National Academy of Sciences, USA **102**, 18225–18230.

Brown BA, Jenkins GI. 2008. UV-B signaling pathways with different fluence-rate response profiles are distinguished in mature Arabidopsis leaf tissue by requirement for UVR8, HY5, and HYH. Plant Physiology **146**, 576–588.

Burchard P, Bilger W, Weissenbock G. 2000. Contribution of hydroxycinnamates and flavonoids to epidermal shielding of UV-A and UV-B radiation in developing rye primary leaves as assessed by ultraviolet-induced chlorophyll fluorescence measurements. Plant, Cell & Environment **23**, 1373–1380.

Chaves I, Pokorny R, Byrdin M, Hoang N, Ritz T, Brettel K, Essen LO, van der Horst GT, Batschauer A, Ahmad M. 2011. The cryptochromes: blue light photoreceptors in plants and animals. Annual Review of Plant Biology **62**, 335–364.

Christie JM, Blackwood L, Petersen J, Sullivan S. 2015. Plant flavoprotein photoreceptors. Plant & Cell Physiology **56**, 401–413.

Davis MB, Shaw RG, Change G, Kareiva PM, Sinauer E, Wang H, Ma L, Li J, Zhao H. 2001. Direct interaction of *Arabidopsis* cryptochromes with COP1 in light control development. Science **294**, 154–158.

Demkura PV, Ballaré CL. 2012. UVR8 mediates UV-B-induced *Arabidopsis* defense responses against *Botrytis cinerea* by controlling sinapate accumulation. Molecular Plant **5**, 642–652.

Döhring T, Köfferlein M, Thiel S, Seidlitz HK. 1996. Spectral shaping of artificial UV-B irradiation for vegetation stress research. Journal of Plant Physiology **148**, 115–119.

Duell-Pfaff N, Wellmann E. 1982. Involvement of phytochrome and a blue light photoreceptor in UV-B induced flavonoid synthesis in parsley (*Petroselinum hortense Hoffm.*) cell suspension cultures. Planta **156**, 213–217.

Favory JJ, Stec A, Gruber H, et al. 2009. Interaction of COP1 and UVR8 regulates UV-B-induced photomorphogenesis and stress acclimation in *Arabidopsis*. The EMBO Journal **28**, 591–601.

Fuglevand G, Jackson JA, Jenkins GI. 1996. UV-B, UV-A, and blue light signal transduction pathways interact synergistically to regulate chalcone synthase gene expression in *Arabidopsis*. The Plant Cell **8**, 2347–2357.

Götz M, Albert A, Stich S, Heller W, Scherb H, Krins A, Langebartels C, Seidlitz HK, Ernst D. 2010. PAR modulation of the UV-dependent levels of flavonoid metabolites in *Arabidopsis thaliana* (L.) Heynh. leaf rosettes: cumulative effects after a whole vegetative growth period. Protoplasma **243**, 95–103.

Gruber H, Heijde M, Heller W, Albert A, Seidlitz HK, Ulm R. 2010. Negative feedback regulation of UV-B-induced photomorphogenesis and stress acclimation in *Arabidopsis*. Proceedings of the National Academy of Sciences, USA **107**, 20132–20137.

Holm S. 1979. A simple sequentially rejective multiple test procedure. Scandinavian Journal of Statistics **6**, 65–70.

Ibdah M, Krins A, Seidlitz HK, Heller W, Strack D, Vogt T. 2002. Spectral dependence of flavonol and betacyanin accumulation in *Mesembryanthemum crystallinum* under enhanced ultraviolet radiation. Plant, Cell & Environment **25**, 1145–1154.

Jenkins GI. 2009. Signal transduction in responses to UV-B radiation. Annual Review of Plant Biology **60**, 407–431.

Jenkins GI. 2017. Photomorphogenic responses to ultraviolet-B light. Plant, Cell & Environment **40**, 2544–2557.

Kliebenstein DJ, Lim JE, Landry LG, Last RL. 2002. Arabidopsis *UVR8* regulates ultraviolet-B signal transduction and tolerance and contains sequence similarity to human *Regulator of Chromatin Condensation 1*. Plant Physiology **130**, 234–243.

Lee J, He K, Stolc V, Lee H, Figueroa P, Gao Y, Tongprasit W, Zhao H, Lee I, Deng XW. 2007. Analysis of transcription factor HY5 genomic binding sites revealed its hierarchical role in light regulation of development. The Plant Cell **19**, 731–749.

Li J, Ou-Lee TM, Raba R, Amundson RG, Last RL. 1993. *Arabidopsis* flavonoid mutants are hypersensitive to UV-B irradiation. The Plant Cell **5**, 171–179.

Lin C. 2000. Plant blue-light receptors. Trends in Plant Science **5**, 337–342.

Lin C, Ahmad M, Gordon D, Cashmore AR. 1995. Expression of an *Arabidopsis* cryptochrome gene in transgenic tobacco results in hypersensitivity to blue, UV-A, and green light. Proceedings of the National Academy of Sciences, USA **92**, 8423–8427.

Lindfors A, Heikkilä A, Kaurola J, Koskela T, Lakkala K. 2009. Reconstruction of solar spectral surface UV irradiances using radiative transfer simulations. Photochemistry and Photobiology **85**, 1233–1239.

Liu CC, Chi C, Jin LJ, Zhu J, Yu JQ, Zhou YH. 2018. The bZip transcription factor *HY5* mediates *CRY1a*-induced anthocyanin biosynthesis in tomato. Plant, Cell & Environment **41**, 1762–1775.

Liu H, Liu B, Zhao C, Pepper M, Lin C. 2011. The action mechanisms of plant cryptochromes. Trends in Plant Science **16**, 684–691.

Mao J, Zhang Y-C, Sang Y, Li Q-H, Yang H-Q. 2005. A role for *Arabidopsis* cryptochromes and COP1 in the regulation of stomatal opening. Proceedings of the National Academy of Sciences, USA **102**, 12270–12275.

Mazzella MA, Cerdán PD, Staneloni RJ, Casal JJ. 2001. Hierarchical coupling of phytochromes and cryptochromes reconciles stability and light modulation of *Arabidopsis* development. Development **128**, 2291–2299.

Morales LO, Brosché M, Vainonen J, Jenkins GI, Wargent JJ, Sipari N, Strid Å, Lindfors AV, Tegelberg R, Aphalo PJ. 2013. Multiple roles for UV RESISTANCE LOCUS8 in regulating gene expression and metabolite accumulation in Arabidopsis under solar ultraviolet radiation. Plant Physiology **161**, 744–759.

Morales LO, Tegelberg R, Brosché M, Keinänen M, Lindfors A, Aphalo PJ. 2010. Effects of solar UV-A and UV-B radiation on gene expression and phenolic accumulation in *Betula pendula* leaves. Tree Physiology **30**, 923–934.

Nawkar GM, Kang CH, Maibam P, et al. 2017. HY5, a positive regulator of light signaling, negatively controls the unfolded protein response in *Arabidopsis*. Proceedings of the National Academy of Sciences, USA **114**, 2084–2089.

Neff MM, Chory J. 1998. Genetic interactions between phytochrome A, phytochrome B, and cryptochrome 1 during Arabidopsis development. Plant Physiology **118**, 27–35.

Neugart S, Rohn S, Schreiner M. 2015. Identification of complex, naturally occurring flavonoid glycosides in *Vicia faba* and *Pisum sativum* leaves by HPLC-DAD-ESI-MSn and the genotypic effect on their flavonoid profile. Food Research International **76**, 114–121.

Oravecz A, Baumann A, Máté Z, Brzezinska A, Molinier J, Oakeley EJ, Adám E, Schäfer E, Nagy F, Ulm R. 2006. CONSTITUTIVELY PHOTOMORPHOGENIC1 is required for the UV-B response in *Arabidopsis*. The Plant Cell **18**, 1975–1990.

OuYang F, Mao J-F, Wang J, Zhang S, Li Y. 2015. Transcriptome analysis reveals that red and blue light regulate growth and phytohormone metabolism in Norway Spruce [*Picea abies* (L.) Karst.]. PLoS One **10**: e0127896.

Pescheck F, Bilger W. 2019. High impact of seasonal temperature changes on acclimation of photoprotection and radiation-induced damage in field grown *Arabidopsis thaliana*. Plant Physiology and Biochemistry **134**, 129–136.

Pinheiro J, Bates D, DebRoy S, Sarkar D; R Core Team. 2018. nlme: Linear and nonlinear mixed effects models. R package version 3.1–137. https://cran.r-project.org/web/packages/nlme/index.html.

R Core Team. 2018. R: A language and environment for statistical computing. Vienna, Austria: R Foundation for Statistical Computing. http://www.R-project.org/.

Rizzini L, Favory JJ, Cloix C, et al. 2011. Perception of UV-B by the *Arabidopsis* UVR8 protein. Science **332**, 103–106.

Schindelin J, Arganda-Carreras I, Frise E, et al. 2012. Fiji: an open-source platform for biological-image analysis. Nature Methods **9**, 676–682.

Schmidt S, Zietz M, Schreiner M, Rohn S, Kroh LW, Krumbein A. 2010. Identification of complex, naturally occurring flavonoid glycosides in kale (*Brassica oleracea var*. sabellica) by high-performance liquid chromatography diode-array detection/electrospray ionization multi-stage mass spectrometry. Rapid Communications in Mass Spectrometry **24**, 2009–2022.

Schoenbohm C, Martens S, Eder C, Forkmann G, Weisshaar B. 2000. Identification of the *Arabidopsis thaliana flavonoid 3'-hydroxylase* gene and functional expression of the encoded P450 enzyme. Biological Chemistry **381**, 749–753.

Siipola SM, Kotilainen T, Sipari N, Morales LO, Lindfors AV, Robson TM, Aphalo PJ. 2015. Epidermal UV-A absorbance and whole-leaf flavonoid composition in pea respond more to solar blue light than to solar UV radiation. Plant, Cell & Environment **38**, 941–952.

Son K-H, Oh M-M. 2013. Leaf shape, growth, and antioxidant phenolic compounds of two lettuce cultivars grown under various combinations of blue and red light-emitting diodes. American Society for Horticultural Science **48**, 988–995.

Stracke R, Favory JJ, Gruber H, Bartelniewoehner L, Bartels S, Binkert M, Funk M, Weisshaar B, Ulm R. 2010. The Arabidopsis bZIP transcription factor HY5 regulates expression of the PFG1/MYB12 gene in response to light and ultraviolet-B radiation. Plant, Cell & Environment **33**, 88–103.

Tevini M, Braun J, Fieser G. 1991. The protective function of the epidermal layer of rye seedlings against ultraviolet-B radiation. Photochemistry and Photobiology **53**, 329–333.

Thiel S, Döhring T, Köfferlein M, Kosak A, Martin P, Seidlitz HK. 1996. A phytotron for plant stress research: how far can artificial lighting compare to natural sunlight? Journal of Plant Physiology **148**, 456–463.

Ulm R, Baumann A, Oravecz A, Máté Z, Adám E, Oakeley EJ, Schäfer E, Nagy F. 2004. Genome-wide analysis of gene expression reveals function of the bZIP transcription factor HY5 in the UV-B response of *Arabidopsis*. Proceedings of the National Academy of Sciences, USA **101**, 1397–1402.

Wade HK, Bibikova TN, Valentine WJ, Jenkins GI. 2001. Interactions within a network of phytochrome, cryptochrome and UV-B phototransduction pathways regulate chalcone synthase gene expression in Arabidopsis leaf tissue. The Plant Journal **25**, 675–685.

Wang F. 2016. SIOX plugin in ImageJ: area measurement made easy. UV4Plants Bulletin **2**, 37–44.

Warnes GR, Bolker B, Lumley T, Johnson RC. 2018. Various R programming tools for model fitting. https://rdrr.io/cran/gmodels/.

Yu X, Liu H, Klejnot J, Lin C. 2010. The cryptochrome blue light receptors. The Arabidopsis Book **8**, e0135.

Zeugner A, Byrdin M, Bouly JP, Bakrim N, Giovani B, Brettel K, Ahmad M. 2005. Light-induced electron transfer in *Arabidopsis* cryptochrome-1 correlates with in vivo function. The Journal of Biological Chemistry **280**, 19437–19440.